ON-CHIP PROCESSOR BASED ON MMI MICRORING RESONATORS FOR IMAGE EDGE DETECTION IN ALL-OPTICAL DOMAIN

Thi Thuy Bui*, The Ngoc Dang*, Trung Thanh Le#
*Posts and Telecommunications Institute of Technology (PTIT), Hanoi, Vietnam
#International School, Vietnam National University (VNU-IS), Hanoi, Vietnam

Abstract: We propose a new optical processor that implement an optical vector matrix multiplication (OVMM) or dot product circuit using multimode interference (MMI) based microring resonator structures. Our structure can be integrated into only one single chip without the need of wavelength division multiplexers (WDM). The control of weight and input signals is based on the graphene material for high speed computing. The proposed architecture provides high bandwidth, controllable accuracy of input signals and weights, high speed, compactness and capacity of working with negative values. The whole device is designed and simulated in Si3N4 platform which can provide a low loss and works directly with visible wavelength range of images. The new architecture can be applied to optical neural networks with high order of connections of neurons for artificial neural networks. We demonstrate the edge detection using Robert, Prewitt and Sobel operators. The speed of processing is up to 28GHz and MSE difference with the conventional method is of order 0.1.

Keywords: All-optical dot product, image processing, multimode interference coupler, optical signal processing

I. INTRODUCTION

In recent years, to deal with the growing demand for faster computation, computing processors such as central processing units (CPUs), graphics processing units (GPUs) and tensor processing units (TPUs) have been extensively developed [1]. However, Moore's law in electronics is approaching the limit and slowing down the speed of data-processing-related improvements. Light recently has been established as a communication medium for telecommunications and data centers for years, but has not been widely utilized in information processing and computing. Photonic integrated circuits (PICs), which manipulate light signals using on-chip optical waveguides, beam couplers, and splitters, electro-optic modulators, photo-detectors, and lasers, etc., have been demonstrated as the platform for a new class of information processing machines to deal with the limits of Moore's law [2]. Leveraging photons instead of electrons for computation, optical processors can provide high-throughput, power-efficient, and low-latency computing performance by overcoming the inherent limitations of electronics. Many application-specific optical processors have been exploited for solving mathematical and signal processing tasks with performance beyond those existing electronic counterparts by orders of magnitude. Optoelectronic components on a PIC platform have flourished due to the capability of transducing signals between light and electricity.

However, for on-chip optical information processing, very few fundamental building blocks equivalent to those used in electronic circuits exist. Optical processor with the task of the dot product is a fundamental operation in modern digital signal processing fields such as digital image processing, radar signal processing and coherent optical communication [3]. In 2012, a new parallel computing method for optical matrix vector multipliers (MVMs) by replacing the fan-out and fan-in with optical lenses by the power splitting and wavelength multiplexing was proposed. This method allows to improve the stability and power efficiency of the system [3].

In the literature, there are some optical methods for the dot product or matrix vector multiplication implementation. The microring resonators (MRRs), microdisk resonators (MDRs), Bragg gratings or Mach–Zehnder interferometers (MZIs) [4, 5] can be used. Two main control methods are based on the thermo-optic effect or the plasma dispersion effect in the optical modulator. Compared with MZIs, the miniaturized size of MRRs makes them a better candidate for large-scale photonic systems since they allow dense on-chip integration for reducing the footprint, power consumption, and cost as well as parallel operations with incoherent light sources. However, for microring resonators, optical directional coupler need to be used [6]. The disadvantage of this structure is the difficulty to achieve extract the desired transmission due to the

Contact author: Thi Thuy Bui
Email: thuyhy87@gmail.com
Manuscript received: 26/6/2022, revised: 22/7/2022, accepted: 06/8/2022.

sensitivity of the coupling ratios to the fabrication. The optical signal modulation is realized by drifting the resonance peak of the MRR modulator. Moreover, the previous structures are difficult to integrate in one single chip due to the requirement of the WDM elements. Therefore, in this study we propose a new microring resonator based on MMI coupler without using directional couplers as shown in the previous research.

With the development of silicon photonics, the silicon photonic based architecture has been shown to perform multiply-accumulate operations at frequencies up to five times faster than conventional electronics [7]. The method employs a bank of tunable silicon MRRs that recreate on-chip synaptic weights. However, the graphene material is particular attract to create the high speed optical devices. The state-of-the-art tuning speed of graphene microring is at 28–80 GHz due to the refractive index of the graphene layer sheet changed by applied voltage into the graphene sheet [8]. On the other hand, the electronic processors have their clock rate limit at around 4–5 GHz as they reach the thermal dissipation limit. Therefore, there is a motivation to explore how photonics could be used to perform convolutions and matrix multiplication. The optical implementation of convolutional neural networks with fast operation speed and high energy efficiency is appealing owing to its outstanding capability of feature extraction and high speed data processing. In particular, convolutional processing based on MVM, which is a computationally intensive operation in electronics, occupies over 80% of the total processing time in convolutional neural networks, therefore computational acceleration for convolutional neural networks can be achieved by matching hardware and MVM operations [9].

In this study, we propose an on-chip optical signal processor performing matrix-vector multiplication with new compact structure without using WDM. Our structures use the graphene so it can provide higher speed up to 28GHz. New microring resonators based on multimode interference coupler are used instead of using microring resonators based on directional couplers. Therefore, all the functional devices can integrated into one single chip. In addition, the coupling ratio of the directional coupler, which is very sensitive to the fabrication tolerance, is not the problem. The first resonance wavelength is controlled by the length of the waveguide. As a result, the resonance wavelength can be achieved accurately. The material Si3N4 platform is used, which is suitable for the existing CMOS technology and has low loss. Our structure can provide a large fabrication tolerance of ±2µm in the length. Such high fabrication tolerance can help the building of the fully-connected network based on the proposed OMMM for novel optical implementation of convolutional neural networks in the future.

II. DESIGN OF THE KERNEL IN ALL-OPTICAL DOMAIN

The proposed structure for the matrix vector multiplication or convolution kernel is shown in Figure 1. The input signal is encoded using the first column array of the MMI based microring resonators and the weight factors or the kernel filter needs no modification because of the unchangeable kernel. Using only this structure, any filter can be created by changing the weight factor through the control of the resonance wavelength as presented in the next section.

Figure 1(a) presents a simple example of convolution computing in image processing. A filter matrix is set for extracting a feature from an input image and applied to a window in the image. The filter and window have the same matrix size, and the sum of their dot products is computed as follows:

$$y_1 = x_1h_1 + x_2h_2 + x_3h_3 + x_4h_4 \quad (1)$$

where x_i (i=1,2,3,4) is the element of the window in the input image and h_i (i=1,2,3,4) is an element of the filter. The filter scans the input image two-dimensionally and product-sums are computed at every spatial position. Then, a convolved feature is finally obtained. For convolving an input matrix with a 2×2 filter, a photonic computing circuit for the product-sum operation is proposed. For Robert's filter applied to the edge detection, $H_x = \begin{bmatrix} +1 & 0 \\ 0 & -1 \end{bmatrix}, H_y = \begin{bmatrix} 0 & +1 \\ -1 & 0 \end{bmatrix}$. As illustrated in Figure 1(b), our proposed architecture comprises four sets of cascaded MMI microring resonators (MRRs) and an 1x4 multimode interference (MMI) coupler with a only single-mode light source. Input signals xi and filter factors hi are the signals that are applied to the first and second MRRs, respectively, after being converted to the driving voltage signals. Each of two MRMs modulates the continuous wave (CW) light from the light source and an optical output from the cascaded MRMs corresponding to a product of xi and hi.

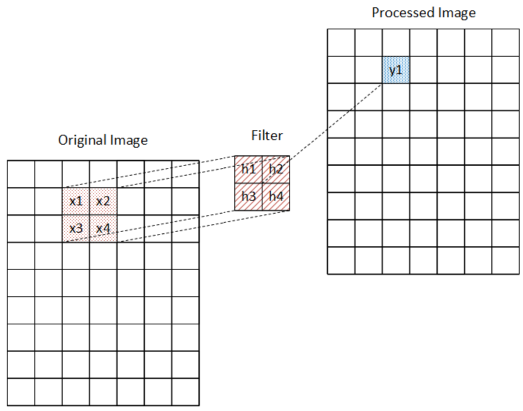

(a)

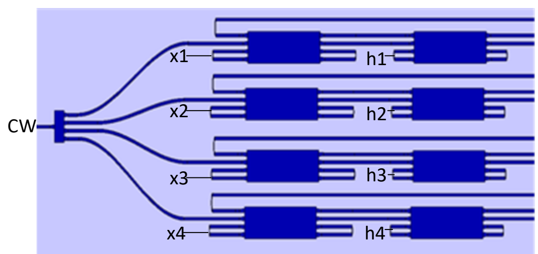

(b)

Figure 1. (a) The image convulution and (b) architecture based on MMI resonators for the dot product implementation

The add-drop microring structure is widely applied in on-chip optical computing owing to the capability of difference processing. Since the power value is non-negative, early work only utilized the through port, then the transmission matrix and the output vector are non-negative, thus the matrix operation is limited in the non-negative number domain. However, fundamental mathematical operations such as matrix–vector multiplication and matrix–matrix multiplication are usually performed in the real number domain in practice. In order to extend the matrix operation to the full real number domain, the final results need to be obtained via the differential processing between the power values of the drop port and the through port; in this way, the transmission matrix and final output vector are both able to contain negative domain. The output intensities at the two ports of the output in the balanced detections can be expressed by

$$I_{out1} = \alpha \sin^2(\frac{\Delta\phi}{2}) I_{in} \quad (2)$$

$$I_{out2} = \alpha \cos^2(\frac{\Delta\phi}{2}) I_{in} \quad (3)$$

where α is the loss factor. As a result the intensity after the balanced photo-detector is $\Delta I = I_{out2} - I_{out1} = \alpha I_{in} \left|\cos(\Delta\phi)\right|$, $\Delta\phi$ is the phase difference in two arms. Therefore, both negative and positive values can be achieved using this proposed method.

In digital image processing, the convolution of an image X with a kernel h produces a convolved image O. An image is represented as a matrix of numbers with dimensionality MxN, where M and N are the height and width of the image, respectively. Each element of a matrix represents the intensity of a pixel at that particular spatial location. A kernel is a matrix of positive or negative numbers with dimensionality R × R. The value of a particular convolved pixel is defined by

$$\begin{aligned} y &= (x_0, x_1, ..., w_R)(h_0, h_1, ..., h_R)^T \\ &= \sum_{k=1}^{R}\sum_{l=1}^{R} x_{k,l} h_{k.l} = \sum_{k=0}^{R-1} \frac{\eta P}{R} T(x_i) T(|h_i|) \end{aligned} \quad (4)$$

where the optical power of the output P is at the balanced circuit; T is the transmissions. The photo-detectors transform the optical powers to current with a photo-electronic efficiency of η. For matrix description, the MVM operation can be mathematically described as

$$Y = hX = \begin{bmatrix} h_{11} & h_{12} & ... & h_{1R} \\ h_{21} & h_{R2} & ... & h_{2R} \\ ... & ... & ... & ... \\ h_{R1} & h_{R2} & ... & h_{RR} \end{bmatrix} \begin{bmatrix} x_1 \\ x_2 \\ ... \\ x_R \end{bmatrix} \quad (5)$$

III. SIMULATION RESULTS AND DISCUSSIONS

A new optical microring resonator based on only one multimode waveguide with four ports is shown in Figure 2. We use Si3N4 waveguide with a width of 1600nm and height of 180nm for input and output waveguides. For a multimode waveguide, we use a wider width of $W_{MMI} = 24\mu m$. In this structure, we use a feedback waveguides for ring waveguides and form the add-drop microring resonator. The drop and through port Tp and Td are shown in Figure 2.

Figure 2. Microring resonator based on only one multimode waveguide structure

In a multimode waveguide, the information of the image position in the x direction and phases of the output images is very important. We need to know where multi-images appear in order to design output waveguides to capture the optical output. Furthermore, phase information of the spot images or output images is important for such devices as MMI switch. It can be shown that the field in the multimode region will be of the form [10]:

$$f(x, L_{MMI}) = \frac{1}{\sqrt{N}} \sum_{p=0}^{N-1} f_{in}(x - x_p) \exp(-j\varphi_p) \quad (6)$$

where $x_p = b(2p - N)\frac{W_{MMI}}{N}$, $\varphi_p = b(N - p)\frac{p\pi}{N}$, $f_{in}(x)$ describes the field profile at the input of the multimode region, x_p and φ_p describe the positions and phases, respectively of N self-images at that output of the multimode waveguide, p denotes the output image number and b describes a multiple of the imaging length. For short device, we choose b=1. Consider a 4x4 multimode waveguide with the length of $L = L_{MMI} = \frac{3L_\pi}{2}$, where $L_\pi = \frac{\pi}{\beta_0 - \beta_1}$ is the beat length of the MMI, β_0, β_1 are the propagation constants of the fundamental and first order modes supported by the multimode waveguide with a width of W_{MMI}. The phases associated with the images from input i to output j can be presented by

$$\begin{aligned} \varphi_{ij} &= -\frac{\pi}{2}(-1)^{i+j+4} \\ &+ \frac{\pi}{16}\left[i + j - i^2 - j^2 + (-1)^{i+j+4}(2ij - i - j + \frac{1}{2})\right] \end{aligned} \quad (7)$$

We showed that the characteristics of an MMI device can be described by a transfer matrix [11]. This transfer matrix is a very useful tool for analysing cascaded MMI structures. The phase ϕ_{ij} associated with imaging an input i to an output j in an MMI coupler. These phases ϕ_{ij} form a matrix S_{4x4}, with i representing the row number, and j representing the column number. A single 4x4 MMI coupler at a length of $L_{MMI} = \frac{3L_\pi}{2}$. The light propagation through the resonator is characterized by a round trip transmission $E_{in,3} = \alpha \exp(j\theta)E_{in,4}$, where $\theta = \frac{2\pi}{\lambda} n_{eff} L_R$ is the round trip phase, α is the loss factor, n_{eff} is the effective refractive index of the SOI single mode waveguide and L_r is the ring resonator circumference. We connect the through and drop ports into the balanced photodiode. The normalized transmitted power at the can be calculated by

$$T_p = \frac{0.5\alpha^2 - \alpha\cos(\varphi) + 0.5}{1 - \alpha\cos(\varphi) + (0.5\alpha)^2} = I_{out1} \tag{8}$$

$$T_d = \frac{0.25\alpha}{1 - \alpha\cos(\varphi) + (0.5\alpha)^2} = I_{out2} \tag{9}$$

In order to obtain the desired factor xi and hi, we use the graphene sheet integrated with Si3N4 waveguide. Graphene can be incorporated into Si3N4 core waveguide to implement graphene silicon nitride waveguide (GSW). The length of the graphene waveguide is L_{arm}. The cross-section view of the graphene silicon waeguide is shown in Figure 3(a). By using the EME (Eigen Mode Expansion) method, the mode profile of the GSW is obtained in Figure 3(b).

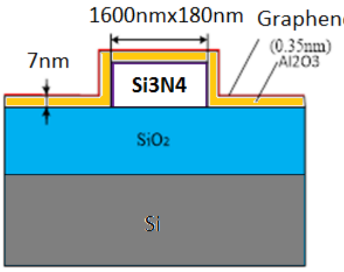

(a)

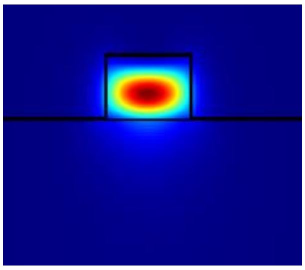

(b)

Figure 3. (a) Waveguide Graphene structure (b) Mode profile

The GSW has a monolayer graphene sheet of 340nm on top of a Si3N4 waveguide, separated from it by a thin Al2O3 layer. Graphene, Al2O3, and silicon together formed a capacitor structure, which was the basic block of the graphene modulator and phase shifter [12]. The presence of the graphene layer changes the propagation characteristics of the guided modes and these can be controlled and reconfigured changing the chemical potential by means of applying a suitable voltage V_g. By using numerical simulations, the real and imaginary parts of the refractive index of graphene with different chemical potentials are shown in Figure 4. Figure 4(c) presents the loss factor at different chemical potentials. Graphene has optical properties due to its band structure that provides both intraband and interband transitions. Both types of the transitions contribute to the material conductivity expressed by [13]:

$$\sigma(\omega) = \sigma_{intra}(\omega) + \sigma_{inter}(\omega) \tag{10}$$

Where $\sigma_{intra}(\omega)$ and $\sigma_{inter}(\omega)$ are the intraband and interband conductivities, which can be calculated by the Kubo's theory:

$$\sigma_{intra}(\omega) = \frac{ie^2}{\pi\hbar(\omega + i2\Gamma)}\left[\frac{\mu_c}{k_B T} + 2\ln(e^{-(\mu_c/k_B T)} + 1)\right] \tag{11}$$

$$\sigma_{inter}(\omega) = -\frac{ie^2}{4\pi\hbar}\ln\left(\frac{2|\mu_c| - (\omega - 2i\Gamma)\hbar}{2|\mu_c| + (\omega - 2i\Gamma)\hbar}\right) \tag{12}$$

Where e is electron charge, $\hbar$ is the angular Planck constant, k_B is the Boltzman constant, T is the temperature, μ_c is the Fermi level or Chemical potential; $\Gamma = \frac{eV_F^2}{\mu\mu_c}$ is the electron collision rate, μ is electron mobility, V_F is the Fermi velocity in graphene.

The dielectric constant of a graphene layer can be calculated by [14, 15]

$$\varepsilon_g(\omega) = 1 + \frac{i\sigma(\omega)}{\omega\varepsilon_0\Delta} \tag{13}$$

The refractive index of the graphene layer sheet can be changed by providing applied voltage V_g to the graphene sheet. It is because it will change the value of the chemical potential:

$$|\mu_c(V_g)| = \hbar V_F\sqrt{\pi|\eta(V_g - V_0)|} \tag{14}$$

Where V_0 is the offset voltage from zero caused by natural doping. Figure 4(b) and (c) presents the effective index of the Si3N4 waveguide for real and imaginary parts depending on the chemical potential.

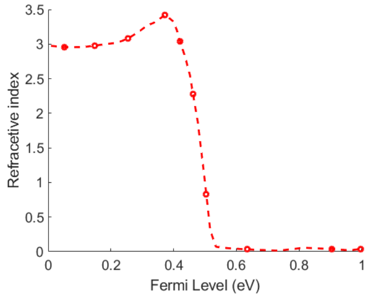

(a)

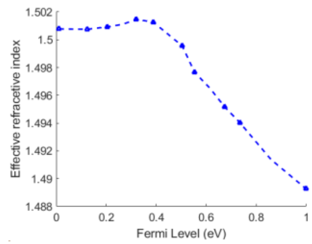

(b)

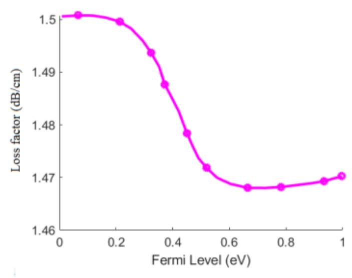

(c)

Figure 4. Effective refractive index of the GSW waveguide

The normalized powers at the through and drop ports of the MMI based resonator are shown in Figure 5(a). The difference power between two port is in the range of (-1, +1) for negative values of the kernel filters. In this simulation, the chemical potential at the graphene is 0.6eV. By controlling the chemical potential we can control the transmission. As a result the desired values of the kernel factor and input image can be obtained. Figure 5(b) presents the normalized transmissions at through, drop and difference for the chemical potential of 0.6eV and 0.65eV. Simulation results show that modulation speed up to 28 GHz. Figure 5(c) shows the transmission difference for different chemical potential. We can see that the positive and negative numbers can be created at one wavelength by controlling the chemical potential.

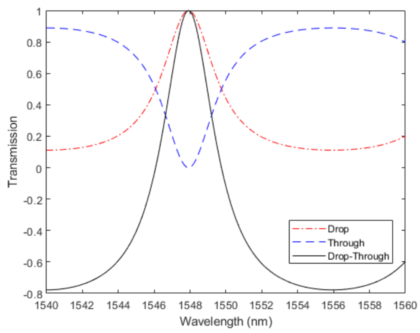

(a)

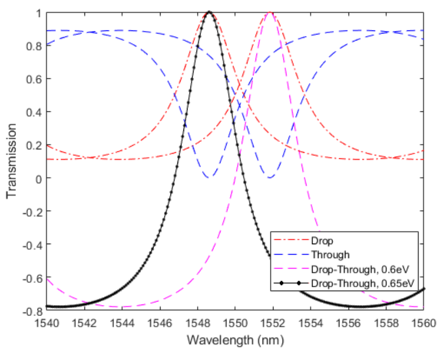

(b)

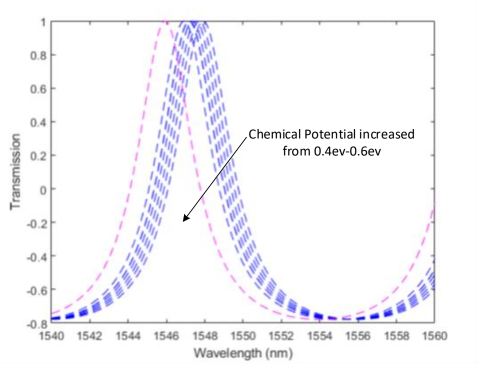

(c)

Figure 5. (a) Normalized transmissions at through and drop ports, (b) the transmissions with two chemical potential and (c) transmissions can be controlled by the change of chemical potenial

The numerical simulation results for signal propagating through the MMI based microring resonator with input signal at port 1 are shown in Figure 6. Figure 6(a) shows the signal propagation for on resonance and Figure 6(b) shows the signal propagation for off resonance. In this study, by controlling the length of the feedback waveguide Lr, we can achieve the fundamental resonance shift. Then by controlling the chemical potential via the applied voltage on the graphene sheet, we can obtain the desired resonance shift. The resonance wavelength is obtained at the resonance condition $m\lambda_r = n_{eff} L_r$, where m is integer numbers.

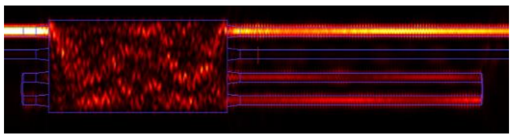

(a)

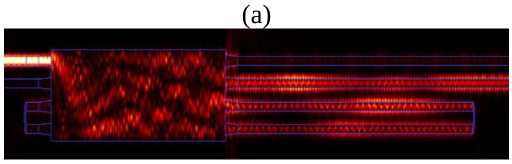

(b)

Figure 6. (a) Signal propagation via the MMI based microring resonator with on resonance and (b) off-resonance

Figure 7 illustrates the signal propagation though the whole structure at different chemical potentials for 0.6eV and 0.65eV. Input signals x1, x2, x3, x4 are changed by controlling the potential chemicals at the MMI resonator for implantation of x1, x2, x3, x4, respectively in Figure 1.

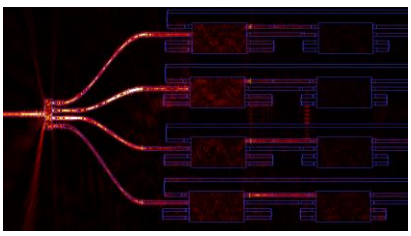

(a)

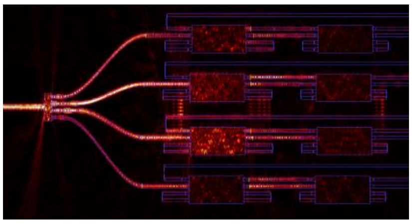

(b)

Figure 7. Signal propagation via the whole device (a) chemical potential 0.6eV and (b) 0.65eV

Now, we verify the working principle of the proposed optical architecture for Robert, Prewitt and Sobel operators. Here we use the modified Sobel operator for representing the value below 1. We use the modified Sobel operator with vertical and horizontal derivative approximations of the following equations:

$$H_x = \frac{1}{2}\begin{bmatrix} -1 & 0 & 1 \\ -2 & 0 & 2 \\ -1 & 0 & 1 \end{bmatrix} \quad (15)$$

$$H_y = \frac{1}{2}\begin{bmatrix} -1 & -2 & -1 \\ 0 & 0 & 0 \\ 1 & 2 & 1 \end{bmatrix} \quad (16)$$

The Prewitt operator:

$$H_x = \begin{bmatrix} -1 & 0 & 1 \\ -1 & 0 & 1 \\ -1 & 0 & 1 \end{bmatrix} \quad (17)$$

$$H_y = \begin{bmatrix} -1 & -1 & -1 \\ 0 & 0 & 0 \\ 1 & 1 & 1 \end{bmatrix} \quad (18)$$

The kernel factors can be achieved by controlling the applied voltages into the graphene sheet as shown above.

The kernel filter h will run from the left to the right, from top to below of the input image as shown in Figure 8 for convolution implementation of the whole image. It is particularly useful for the proposed structure that the hardware architecture requires no change for implementing the edge detection operators. We only need to change the applied voltage at the graphene sheet to change the chemical potential. The speed of the graphene change is very fast, so the processing speed of the device is also very high.

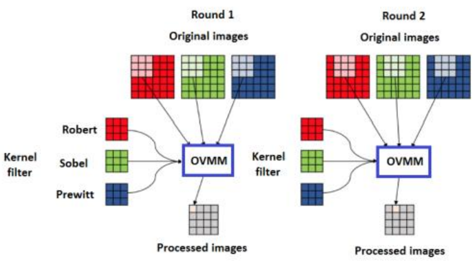

Figure 8. Algorithm for image convolution computation using three kernel operators on the same hardware

(a) Edge detection, MNIST dataset

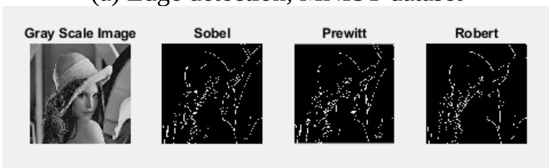

(b) Edge detection, Lena image

Figure 9. Edge detection using the proposed OVMM (a) MNIST dataset and (b) Lena

As examples, we use the MNIST (Modified National Institute of Standards and Technology database) dataset and Lena images for verifying the working principle of the proposed architecture. Figure 9 shows the gray image of the MNIST dataset for number 4 as an example. The edge detection with three operators are shown in Figure 9(a). Figure 9(b) shows the results of the edge detection of Lena image using three designed operators. The difference between the proposed OVMM and SciPy was quantified by taking the mean squared error (MSE) of each of the output pixels of 0.1. The MSE difference is shown in Figure 10. The MSE of the image is calculated by

$$MSE = \frac{1}{MxN}\sum_{i=0}^{M-1}\sum_{j=0}^{N-1}[x(i,j) - y_{OVMM}(i,j)]^2 \quad (19)$$

Where the output pixel(i,j) calculated by the OVMM $y_{OVMM}(i,j)$. The difference in MSE between the image processed by the OVMM and Scipy is expressed by

$$\Delta MSE = \left|\frac{1}{MxN}\sum_{i=0}^{M-1}\sum_{j=0}^{N-1}[x(i,j) - y_{OVMM}(i,j)]^2\right| - \left|\frac{1}{MxN}\sum_{i=0}^{M-1}\sum_{j=0}^{N-1}[x(i,j) - y_{Scipy}(i,j)]^2\right| \quad (20)$$

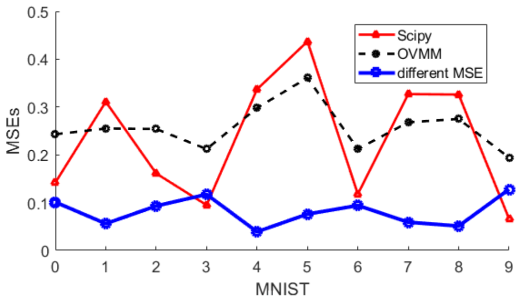

Figure 10. The MSE using the proposed OVMM and Scipy for MNIST dataset

IV. CONCLUSION

A new optical processor that implement an optical vector matrix multiplication (OVMM) circuit using multimode interference (MMI) structures has been proposed in this study. The high speed of 28GHz has been obtained by using graphene on the Si3N4 waveguide. The proposed structure use only MMI coupler with feedback waveguides. The advantages of the proposed structure is no need of the WDM elements, high fabrication tolerance for high accuracy computing, compactness, low loss. The new architecture can be applied to optical neural networks with high order of connections of neurons for artificial neural networks with low loss and ultra-wideband. We demonstrate the edge detection using Robert, Prewitt and Sobel operators with the MSE difference with the SciPy in the order of 0.1.

REFERENCES

[1] S. Xiang *et al.*, "A review: Photonics devices, architectures, and algorithms for optical neural computing," *Journal of Semiconductors,* vol. 42, no. 2, p. 023105, 2021/02/01 2021, doi: 10.1088/1674-4926/42/2/023105.

[2] X. Sui, Q. Wu, J. Liu, Q. Chen, and G. Gu, "A Review of Optical Neural Networks," *IEEE Access,* vol. 8, pp. 70773-70783, 2020, doi: 10.1109/ACCESS.2020.2987333.

[3] L. Yang, R. Ji, L. Zhang, J. Ding, and Q. Xu, "On-chip CMOS-compatible optical signal processor," *Optics Express,* vol. 20, no. 12, pp. 13560-13565, 2012/06/04 2012, doi: 10.1364/OE.20.013560.

[4] M. Salmani, A. Eshaghi, E. Luan, and S. Saha, "Photonic computing to accelerate data processing in wireless communications," *Optics Express*, vol. 29, no. 14, pp. 22299-22314, 2021/07/05 2021, doi: 10.1364/OE.423747.

[5] N. C. Harris *et al.*, "Linear programmable nanophotonic processors," *Optica,* vol. 5, no. 12, pp. 1623-1631, 2018/12/20 2018, doi: 10.1364/OPTICA.5.001623.

[6] T. T. Le, L. W. Cahill, and D. Elton, "The Design of 2x2 SOI MMI couplers with arbitrary power coupling ratios," *Electronics Letters,* vol. 45, no. 22, pp. 1118-1119, 2009.

[7] A. N. Tait, M. A. Nahmias, B. J. Shastri, and P. R. Prucnal, "Broadcast and Weight: An Integrated Network For Scalable Photonic Spike Processing," *Journal of Lightwave Technology,* vol. 32, no. 21, pp. 4029-4041, 2014, doi: 10.1109/JLT.2014.2345652.

[8] J. Liu, Z. U. Khan, C. Wang, H. Zhang, and S. Sarjoghian, "Review of graphene modulators from the low to the high figure of merits," *Journal of Physics D: Applied Physics,* vol. 53, no. 23, p. 233002, 2020/04/03 2020, doi: 10.1088/1361-6463/ab7cf6.

[9] X. Xu *et al.*, "11 TOPS photonic convolutional accelerator for optical neural networks," *Nature,* vol. 589, no. 7840, pp. 44-51, 2021/01/01 2021, doi: 10.1038/s41586-020-03063-0.

[10] M. Bachmann, P. A. Besse, and H. Melchior, "General self-imaging properties in N x N multimode interference couplers including phase relations," *Appl. Opt.*, vol. 33, no. 18, pp. 3905-, 1994.

[11] T.-T. Le, *Multimode Interference Structures for Photonic Signal Processing*. LAP Lambert Academic Publishing, 2010.

[12] Q. Bao, *2D Materials for Photonic and Optoelectronic Applications*. Woodhead Publishing, 2019.

[13] P. Xing, K. J. A. Ooi, and D. T. H. Tan, "Ultra-broadband and compact graphene-on-silicon integrated waveguide mode filters," *Scientific Reports,* vol. 8, no. 1, p. 9874, 2018, doi: 10.1038/s41598-018-28076-8.

[14] G. W. Hanson, "Dyadic Green's functions and guided surface waves for a surface conductivity model of graphene," *Journal of Applied Physics,* vol. 103, no. 6, p. 064302, 2008, doi: 10.1063/1.2891452.

[15] J. Capmany, D. Domenech, and P. Muñoz, "Silicon graphene Bragg gratings," *Optics Express,* vol. 22, no. 5, pp. 5283-5290, 2014, doi: 10.1364/OE.22.005283.

BỘ XỬ LÝ TRÊN CHIP DỰA TRÊN VI CỘNG HƯỞNG MMI CHO ỨNG DỤNG TÁCH BIÊN ẢNH TRONG MIỀN QUANG

Tóm tắt: Bài báo thiết kế bộ xử lý quang thực hiện phép nhân chập vector dựa vào cấu trúc giao thoa đa mode và vi cộng hưởng. Cấu trúc mới có thể được tích hợp trên một chip do không cần sử dụng các bộ ghép bước sóng như trước đây. Các trọng số của bộ lọc nhân và tín hiệu được mã hóa và điều chế dựa vào sự thay đổi điện áp của graphene. Điều này cung cấp cho cấu trúc mới có tốc độ cao, điều khiển được hệ số chính xác, nhỏ gọn và đặc biệt có thể làm việc với hệ số bộ lọc kernel âm. Toàn bộ cấu trúc mới được thiết kế trên nền vật liệu Si3N4 có thể làm việc tại các bước sóng nhìn thấy phù hợp với ảnh số. Kiến trúc mới sau đó được áp dụng để thực hiện các toán tử Sobel, Prewitt và Robert trong miền quang để tách biên ảnh. Kết quả cho thấy tốc độ xử lý cao gấp 5 lần, tương ứng 28GHz so với bình thường. Kết quả tách biên ảnh được so sánh với Scipy cho thấy sai khác MSE cỡ 0,1.

Từ khóa: Nhân chập toàn quang, xử lý ảnh, giao thoa đa mode, xử lý tín hiệu quang.

Thi Thuy Bui is the lecturer at Hanoi University of Natural Resources and Environment, Hanoi, Vietnam. She is pursuiting the PhD in computer engineering at Posts and Telecommunications Institute of Technology (PTIT), Hanoi, Vietnam.

Email: thuyhy87@gmail.com

The Ngoc Dang, Associate Professor, Vice Dean of Telecommunications Faculty, Head of Wireless Communications Department, Optical Communications Research Group at Posts & Telecommunications Institute of Technology (PTIT).

Trung Thanh Le, Associate Professor, PhD in electronic and telecommunicaton engineering at Vietnam National University (VNU), Hanoi, Vietnam. He is now the research leader of the team on optical integrated circuits at International School of VNU and Rector of the International School. He got the PhD degree from La Trobe University, Australia in 2009.

Email: thanh.le@vnu.edu.vn